International Journal of Innovative Technology and Exploring Engineering (IJITEE)
ISSN: 2278-3075 (Online), Volume-14 Issue-7, June 2025

A Novel PSO-Gain Super-Twisting Integral Sliding Mode Controller for Sensor-Less Speed Control of Saturated DFIM

PABAME Frédéric, NFAH MBAKA Eustace

Abstract*: This work deals with the performance and optimisation of the speed control of a doubly fed asynchronous machine (DFIM), modelled considering the magnetic circuit's saturation. The speed control strategy of the machine, thus implemented, is a super twisting algorithm with integral action, consisting of five regulators: four for stator and rotor currents, and one for speed regulation. The control was achieved without a mechanical sensor, thanks to an observer that reconstructs the machine's rotation speed from the readings of the currents and voltages it absorbs. The coefficients of the regulators and those of the observer were determined by the Particle Swarm Optimisation (PSO) methods. Thus, the system's efficiency was tested and validated across several speed ranges, including very low speeds, low speeds, and high speeds, using the MATLAB/Simulink simulation software. The control system's performance was demonstrated by varying the set speed according to a predefined profile. The resistive torque and the rotor and stator resistances values were modified by up to 50% to demonstrate the insensitivity to disturbances or variations in the machine parameters.

***Keywords*: DFIM, Saturated Magnetic Circuit, PSO, Sliding Mode, Super-Twisting, Integral Action, Observer.**

Abbreviations:
DFIM: Doubly Fed Induction Machine
PSO: Particle Swarm Optimisation
ST: Super-Twisting

Nomenclature

I_{sd}, $i_{sq,}$	*Stator current*
i_{rd}, i_{rq}	*Rotor current*
v_{sd}, $v_{sq,}$	*Stator voltage*
v_{rd}, v_{rq}	*Rotor voltage*
R_s	*Stator résistance*
R_r	*Rotor résistance*
L_s	*Stator inductance*
L_r	*Rotor inductance*
M_{sr}	*Mutual inductance*
C_{em}	*Electromagnetic torque*

C_r	*Resistant torque*
J	*Moment of inertia*
f	*Coefficients of friction*
w	*Angular velocity*
	Stator self-inductance
$l_{\sigma r}$	*Rotor self-inductance*
	flux

Manuscript received on 18 April 2025 | First Revised Manuscript received on 25 April 2025 | Second Revised Manuscript received on 17 May 2025 | Manuscript Accepted on 15 June 2025 | Manuscript published on 30 June 2025.
*Correspondence Author(s)
PABAME Frederic*, Department of Physics, Faculty of Sciences, University of Dschang, Cameroon Email ID: fredericpabame@yahoo.fr, ORCID ID: 0009-0007-2763-0984
NFAH MBAKA Eustace, Department of Physics, University of Dschang, IUT Fotso Victor, Bandjoun, Cameroon Email ID: emnfah@yahoo.fr, ORCID ID: 0000-0001-9588-3245

I. NTRODUCTION

The doubly-fed induction machines (DFIM) play a crucial role in modern industrial systems, particularly in the fields of wind energy and variable speed drives [1]. Their ability to operate at variable speeds with high energy efficiency makes them essential components for applications requiring precise speed regulation [2]. However, the complexity of their nonlinear dynamics, accentuated by magnetic saturation effects, makes their control particularly challenging. In addition, the use of mechanical sensors to measure speed increases costs and reduces system reliability, motivating the development of sensorless speed control techniques [3].

Among the robust control methods, sliding mode control has proven effective in managing nonlinear and uncertain systems [4]. The Super-Twisting (ST) technique, an advanced variant of sliding mode control, offers a significant reduction in chatter while maintaining high robustness to disturbances and parametric variations [5]. Incorporating integral action into this technique improves control accuracy by eliminating static errors [6]. However, to optimise the performance of this approach, it is necessary to fine-tune the controller parameters. This is where particle swarm optimisation (PSO) comes in, a metaheuristic method inspired by collective intelligence, capable of finding optimal solutions in complex spaces [7].

In this paper, we propose a sensorless speed control strategy for a saturated doubly fed three-phase induction machine based on the Super-Twisting technique with integral action optimised by the particle swarm method. This approach aims to ensure robust and accurate speed control while accounting for magnetic saturation effects and eliminating the need for mechanical sensors. We present a detailed modelling of the saturated DFIM, followed by the design of the control law, the synthesis of an observer to reconstruct the mechanical speed of the machine, and the optimisation of the controller and observer parameters with PSO. Simulation results are also provided to validate the effectiveness of the proposed method.

This study contributes to the advancement of sensorless control techniques for doubly fed induction machines, providing a robust and optimised solution for demanding industrial applications.

II. METHODOLOGY

A. Modelling of the DFIM

With the aim of efficient control for the DFIM, the modelling requires an accurate model that reflects its dynamic behaviour. An adequate model is chosen by taking the (*d-q*) reference frame with an oriented rotor flux as illustrated in [8].

The electrical equations of the machine in the (*d-q*) reference frame are given by the following relations.

$$\begin{cases} U_{sd} = R_s i_{sd} + \dfrac{d\varphi_{sd}}{dt} - \omega_s \varphi_{sq} \\ U_{sq} = R_s i_{sq} + \dfrac{d\varphi_{sq}}{dt} + \omega_s \varphi_{sd} \\ U_{rd} = R_r i_{rd} + \dfrac{d\varphi_{rd}}{dt} - (\omega_s - \omega_r)\varphi_{rq} \\ U_{rq} = R_r i_{rq} + \dfrac{d\varphi_{rq}}{dt} + (\omega_s - \omega_r)\varphi_{rd} \end{cases} \quad \dots \quad (1)$$

In these equations, fluxes are a function of inductances, and inductance values vary according to magnetising currents. The following relationship gives the magnetising currents in the machine [9]

$$i_{md} = i_{sd} + i_{rd} \quad \dots \quad (2)$$

$$i_{mq} = i_{sq} + i_{rq} \quad \dots \quad (3)$$

We derive the total magnetising current as follows.

$$i_m = \sqrt{{i_{md}}^2 + {i_{mq}}^2} \quad \dots \quad (4)$$

The inductances in the machine can be broken down into two parts: the self-inductances l_σ due to the influence of the coil through which the current flows, and the mutual inductances *Msr* due to the influence of neighbouring coils. From where the total inductance in a branch is given as follows

$$l_s(i_m) = l_{\sigma s}(i_m) + M(i_m) \quad \dots \quad (5)$$

$$l_r(i_m) = l_{\sigma r}(i_m) + M(i_m) \quad \dots \quad (6)$$

In this work, inductance values are determined experimentally and approximated by polynomial functions as presented in Refs [10]

$$l_{\sigma s}(i_m) = -2.6e^{-9}{i_m}^3 - 1.8e^{-7}{i_m}^2 - 4.9e^{-5}i_m + 0.38\ [mH] \quad \dots \quad (7)$$

$$l_{\sigma r}(i_m) = -8.7e^{-10}{i_m}^3 - 5.1e^{-8}{i_m}^2 - 1.6e^{-5}i_m + 0.12\ [mH] \quad \dots \quad (8)$$

$$M(i_m) = 1.2e^{-14}{i_m}^7 - 8.4e^{-12}{i_m}^6 + 2.1e^{-9}{i_m}^5 + 2e^{-7}{i_m}^4 - 6.2e^{-6}{i_m}^3 - 1.7e^{-4}{i_m}^2 + 2.9e^{-4}i_m + 8.3\ [mH] \quad \dots \quad (9)$$

The equations for inductance-dependent fluxes are as follows.

$$\begin{aligned} \varphi_{sd} &= l_s(i_m)i_{sd} + M_{sr}(i_m)i_{rd} \\ \varphi_{sq} &= l_s(i_m)i_{sq} + M_{sr}(i_m)i_{rq} \\ \varphi_{rd} &= l_r(i_m)i_{rd} + M_{sr}(i_m)i_{sd} \\ \varphi_{rq} &= l_r(i_m)i_{rq} + M_{sr}(i_m)i_{sq} \end{aligned} \quad \dots \quad (10)$$

The electromagnetic torque is given by

$$C_{em} = mJ\left(\varphi_{rd} i_{sq} - \varphi_{rq} i_{sd}\right) \quad \dots \quad (11)$$

The mechanical equation is given by

$$C_{em} - C_r = J\frac{d\omega}{dt} + f\omega \quad \dots \quad (12)$$

The following system gives the current dynamics of the machine.

$$\begin{cases} \dfrac{di_{sd}}{dt} = -\gamma i_{sd} + \omega_s i_{sq} + ba\varphi_{rd} + bp\omega\varphi_{rq} + m_1 v_{sd} - bv_{rd} \\ \dfrac{di_{sq}}{dt} = -\gamma i_{sq} - \omega_s i_{sd} - bp\omega\varphi_{rd} + ba\varphi_{rq} + m_1 v_{sq} - bv_{rq} \\ \dfrac{di_{rd}}{dt} = -\gamma_1 i_{rd} + (\omega_s - p\omega)i_{rq} + ba_1\varphi_{sd} - bp\omega\varphi_{sq} - bv_{sd} + m_2 v_{rd} \\ \dfrac{di_{rq}}{dt} = -\gamma_1 i_{rq} - (\omega_s - p\omega)i_{rd} + ba_1\varphi_{sq} + bp\omega\varphi_{sd} - bv_{sq} + m_2 v_{rq} \\ \dfrac{d\varphi_{sd}}{dt} = a_1 M_{sr} i_{rd} - a_1\varphi_{sd} + \omega_s\varphi_{sq} + v_{sd} \\ \dfrac{d\varphi_{sq}}{dt} = a_1 M_{sr} i_{rq} - a_1\varphi_{sq} - \omega_s\varphi_{sd} + v_{sq} \\ \dfrac{d\varphi_{rd}}{dt} = aM_{sr} i_{sd} - a\varphi_{rd} + (\omega_s - p\omega)\varphi_{rq} + v_{rd} \\ \dfrac{d\varphi_{rq}}{dt} = aM_{sr} i_{sq} - (\omega_s - p\omega)\varphi_{rd} + v_{rq} \\ \dfrac{d\omega}{dt} = m\varphi_{rd} i_{sq} - \dfrac{C}{J}\omega - \dfrac{Tl}{J} \end{cases} \quad \dots \quad (13)$$

Where

$$\begin{cases} m_1 = \dfrac{1}{\sigma l_s} \\ b = \dfrac{M_{sr}}{\sigma l_s l_r} \\ a = \dfrac{R_r}{l_r} \\ \gamma = \dfrac{R_s l_r^2 + R_r M_{rs}^2}{\sigma l_r l_s} \\ a_1 = \dfrac{R_s}{l_s} \\ \gamma_1 = \dfrac{R_r l_s^2 + R_s M_{rs}^2}{\sigma l_r l_s} \\ m_2 = \dfrac{1}{\sigma l_r} \\ \sigma = \dfrac{1 - M_{sr}^2}{l_s l_r} \end{cases} \quad \dots \quad (14)$$

Table-I: Characteristics of the Machine

Parameters	values
Rs	0.007Ω
Rr	0.007 Ω
p	2
f	0.9
J	0.541
Rated power	660kVA
Ωn	1440Tr/min
Rated voltage	460v
Rated frequency	60Hz

B. Theory of Sliding Mode Control

Sliding mode control is well-documented in the literature, and the basic principles are thoroughly explained in [11]. In this section, we will review the sliding mode to introduce super twisting with integral action.

Published By:
Blue Eyes Intelligence Engineering
and Sciences Publication (BEIESP)

The classical sliding mode is designed in two steps: the first consists of converging the system towards the sliding surface (S = 0) in a finite time for relative degrees of order 1, called discontinuous control. The second consists of maintaining the system on the sliding surface. The control law appears explicitly in the expression of the derivative of the sliding surface ($\dot{S} = 0$) called equivalent control. The total control law is thus the sum of the discontinuous control and the equivalent control. When the states of the system reach the sliding surface, they become insensitive to delimited external disturbances. At this moment, the dynamics of the system are known as the dynamics of the sliding mode. Initially, during the design, it is necessary to predict the dynamic structure of the sliding mode and then design the sliding surface to stabilise it [12]. The dynamics of the sliding mode are generally asymptotically stabilised.

The main disadvantage of the classical sliding mode is the chattering phenomenon, which is characterised by small oscillations of the system output around the setpoint. This is due to discontinuous control, which is generally implemented using the "Sign" function. It can also be due to digital implementation problems. These oscillations are very harmful to the power of motion systems. Solutions exist in the literature. The "Sat" function often replaces the "Sign" function, but this solution is not practical for some applications because the system loses its robustness and accuracy in the face of disturbances [13]. The chattering phenomenon is corrected by applying the higher-order sliding mode developed by [14]. If we consider, for example, a system whose output dynamics is of class S, where r is the degree of relative state of the system. The successive derivatives S ($\dot{S}, \ddot{S}, \ldots, S^{r-1}$) are the continuous functions of the state of the system or the set $\dot{S} = \ddot{S} = \cdots = S^{r-1} = 0$ is non-empty and locally consists of Filippov trajectories. The motion on the set mentioned above is said to exist in r-sliding mode or r-order sliding mode. The r-derivative S^r is discontinuous or non-existent. Therefore, the high-order sliding mode removes the relative degree restriction and can practically eliminate the chattering problem. There are several higher-order sliding mode algorithms among which we can cite: sub-optimal controller, the terminal sliding mode controllers, the twisting controller, and the super-twisting controller. Super-twisting is preferable to twisting because it does not require knowledge of the derivative of the sliding surface.$\dot{S}$. In this work, we will converge the system toward a slip plane that is easier to reach than a slip surface. Once arrived, it will be difficult to escape.
Let the equation give a system.

$$\dot{x} = f(x,t) + u \quad \ldots \quad (15)$$

The control law of super twisting is given by

$$u = -k_1\sqrt{|s|}sign(s) + v \quad \ldots \quad (16)$$

$$\dot{v} = -k_2 sign(s) \qquad (17)$$

S being the sliding surface of the finished product.

$$s = e + w\int e\,dt \quad \ldots \quad (18)$$

e being the difference between the desired state and the current state of a variable of the system. The dynamics of the system (19) is given by

$$\dot{x} = -k_1\sqrt{|s|}sign(s) + v + f(x,t) \quad \ldots \quad (19)$$

The stability of the system is verified by the Lyapunov function and given by the following equation:

$$V = 2k_2|e| + \frac{1}{2}v^2 + \frac{1}{2}(k_1\sqrt{|e|}sign(e) - v)^2 \quad \ldots \quad (20)$$

C. PSO-Gain Super-Twisting Integral Sliding Mode Controller for Speed Control of Saturated DFIM

Flux-oriented control consists of orienting the flux along the d-axis of the rotating reference frame to simplify the model expression. As a result, control of the induction machine becomes analogous to that of a separately excited DC machine.

After orientation along the d-axis, the components of the flux along the q-axis cancel each other out. $\varphi_{rq} = o$, and the electromagnetic torque becomes

$$C_{em} = mJ\varphi_{rd}i_{sq} \quad \ldots \quad (21)$$

To impose the rotor flux modulus, we will magnetise the machine through the stator, resulting in

$$i_{rd} = o \quad \ldots \quad (22)$$

$$i_{rq} = \frac{M_{sr}}{L_r}\, i_{sq} \quad \ldots \quad (23)$$

Thus, the model of the oriented flux machine is given by the following equations.

$$\begin{cases} U_{sd} = R_s i_{sd} + \dfrac{d\varphi_{sd}}{dt} - \omega_s\varphi_{sq} \\ U_{sq} = R_s i_{sq} + \dfrac{d\varphi_{sq}}{dt} + \omega_s\varphi_{sd} \\ U_{rd} = R_r i_{rd} + \dfrac{d\varphi_{rd}}{dt} \\ U_{rq} = R_r i_{rq} + \dfrac{d\varphi_{rq}}{dt} + (\omega_s - \omega_r)\varphi_{rd} \end{cases} \quad \ldots \quad (24)$$

$$\begin{cases} \dfrac{di_{sd}}{dt} = -\gamma i_{sd} + \omega_s i_{sq} + ba\varphi_{rd} + m_1 v_{sd} - bv_{rd} \\ \dfrac{di_{sq}}{dt} = -\gamma i_{sq} - \omega_s i_{sd} - bp\omega\varphi_{rd} + m_1 v_{sq} - bv_{rq} \\ \dfrac{di_{rd}}{dt} = -\gamma_1 i_{rd} + (\omega_s - p\omega)i_{rq} + ba_1\varphi_{sd} - bp\omega\varphi_{sq} - bv_{sd} + m_2 v_{rd} \\ \dfrac{di_{rq}}{dt} = -\gamma_1 i_{rq} - (\omega_s - p\omega)i_{rd} + ba_1\varphi_{sq} + bp\omega\varphi_{sd} - bv_{sq} + m_2 v_{rq} \\ \dfrac{d\omega}{dt} = m\varphi_{rd}i_{sq} - \dfrac{C}{J}\omega - \dfrac{Tl}{J} \end{cases} \quad (25)$$

The following system of equations gives the dynamics of the machine.

From equation 24, we define the new voltages for

Published By:
Blue Eyes Intelligence Engineering
and Sciences Publication (BEIESP)

each current differential equation.

$$\begin{cases} v_{1sd} = m_1 v_{sd} - b v_{rd} \\ v_{1rd} = -b v_{sd} + m_2 v_{rd} \end{cases} \quad \dots \quad (26)$$

$$\begin{cases} v_{1rq} = -b v_{sq} + m_2 v_{rq} \\ v_{1sq} = m_1 v_{sq} - b v_{rq} \end{cases} \quad \dots \quad (27)$$

From these new tensions, equation 24 becomes

$$\begin{cases} \dfrac{di_{sd}}{dt} = -\gamma_{sd} i_{sd} + \omega_s i_{sq} + ba\varphi_{rd} + v_{1sd} \\ \dfrac{di_{sq}}{dt} = -\gamma_{sq} i_{sq} - \omega_s i_{sd} - bp\omega\varphi_{rd} + v_{1sq} \\ \dfrac{di_{rd}}{dt} = -\gamma_1 i_{rd} + (\omega_s - p\omega) i_{rq} + ba_1\varphi_{sd} - bp\omega\varphi_{sq} + v_{1rd} \\ \dfrac{di_{rq}}{dt} = -\gamma_1 i_{rq} - (\omega_s - p\omega) i_{rd} + ba_1\varphi_{sq} + bp\omega\varphi_{sd} + v_{1sq} \\ \dfrac{d\omega}{dt} = \dfrac{1}{J} C_{em} - \dfrac{C}{J}\omega - \dfrac{Tl}{J} \end{cases} \quad \dots \quad (28)$$

The control system will consist of five controllers, one for each of the four currents and one for the speed. The reference currents are obtained by an estimator that takes the electromagnetic torque and the reference flux as input. The estimator is designed based on the control law and the equations derived from the flux orientation.

$$\begin{cases} i_{sd}^{ref} = \dfrac{1}{M_{sr}} \varphi_{rd}^{ref} \\ i_{sq}^{ref} = \dfrac{l_r}{p M_{sr} \varphi_{rd}^{ref}} C_{em}^{ref} \\ i_{rd}^{ref} = 0 \\ i_{rq}^{ref} = -\dfrac{1}{p\varphi_{rd}^{ref}} C_{em}^{ref} \end{cases} \quad \dots \quad (29)$$

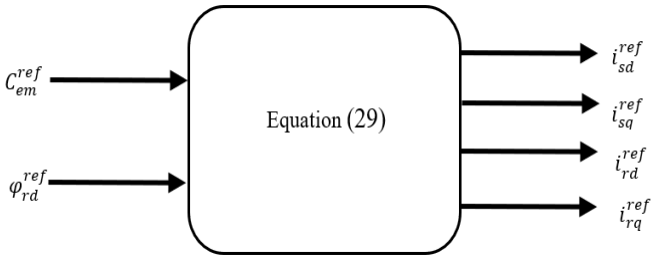

[Fig.1: Reference Current Estimator]

The reference electromagnetic torque is obtained by the speed regulator. The synchronous pulsation is also obtained from the equations resulting from the flux orientation. From equation (13), we can deduce the expression for ω_s

$$\omega_s = \mathrm{p}\omega + \frac{aM_s i_{sq}}{\varphi_{rd}} + \frac{v_{rq}}{\varphi_{rd}} \quad \dots \quad (30)$$

From the machine dynamics (equation 24), we define five sliding surfaces in two ways. The first one is the ordinary super-twisting, and the second one is the integral super-twisting.

$$\begin{cases} s_{isd} = e_{isd} \\ s_{isq} = e_{isq} \\ s_{ird} = e_{ird} \\ s_{irq} = e_{irq} \\ s_{\omega} = e_{\omega} \end{cases} \quad \dots \quad (31)$$

$$\begin{cases} s_{isd} = e_{isd} + k_1 \int e_{isd} dt \\ s_{isq} = e_{isq} + k_2 \int e_{isq} dt \\ s_{ird} = e_{ird} + k_3 \int e_{ird} dt \\ s_{irq} = e_{irq} + k_4 \int e_{irq} dt \\ s_{\omega} = e_{\omega} + k_5 \int e_{\omega} dt \end{cases} \quad \dots \quad (32)$$

$$\text{With} \quad \begin{cases} e_{isd} = i_{sd} - i_{sd}^{ref} \\ e_{isq} = i_{sq} - i_{sq}^{ref} \\ e_{ird} = i_{sd} - i_{sd}^{ref} \\ e_{irq} = i_{rd} - i_{rd}^{ref} \\ e_{\omega} = i_{\omega} - i_{\omega}^{ref} \end{cases} \quad \dots \quad (33)$$

The following equations give the derivatives of the sliding surfaces:

$$\begin{cases} \dot{s}_{isd} = f_1(i_{sd}) + v_{1sd} - i_{sd}^{ref} + k_1 e_{isd} \\ \dot{s}_{isq} = f_2(i_{sq}) + v_{1sq} - i_{sq}^{ref} + k_2 e_{isq} \\ \dot{s}_{ird} = f_3(i_{rd}) + v_{1rd} - i_{rd}^{ref} + k_3 e_{ird} \\ \dot{s}_{irq} = f_4(i_{rq}) + v_{1rq} - i_{rq}^{ref} + k_4 e_{irq} \\ \dot{s}_{\omega} = f_5(\omega) + \dfrac{1}{J} C_{em} - \dot{\omega}^{ref} + k_5 e_{\omega} \end{cases} \quad \dots \quad (34)$$

With

$$\begin{cases} f_1(i_{sd}) = -\gamma i_{sd} + \omega_s i_{sq} + ba\varphi_{rd} \\ f_2(i_{sq}) = -\gamma i_{sq} - \omega_s i_{sd} - bp\omega\varphi_{rd} \\ f_3(i_{rd}) = -\gamma_1 i_{rd} + (\omega_s - p\omega) i_{rq} + ba_1\varphi_{sd} - bp\omega\varphi_{sq} \\ f_4(i_{rq}) = -\gamma_1 i_{rq} - (\omega_s - p\omega) i_{rd} + ba_1\varphi_{sq} + bp\omega\varphi_{sd} \\ f_5(\omega) = -\dfrac{C}{J}\omega - \dfrac{Tl}{J} \end{cases} \quad \dots \quad (35)$$

These equations can be rewritten in the following form:

$$\begin{cases} \dot{s}_{isd} = \emptyset_1(i_{sd}) + v_{1sd} \\ \dot{s}_{isq} = \emptyset_{sq}(i_{sq}) + v_{1sq} \\ \dot{s}_{ird} = \emptyset_{rd}(i_{rd}) + v_{1rd} \\ \dot{s}_{irq} = \emptyset_{rq}(i_{rq}) + v_{1rq} \\ \dot{s}_{\omega} = \emptyset_{\omega}(\omega) + \dfrac{1}{J} C_{em} \end{cases} \quad \dots \quad (36)$$

With

$$\begin{cases} \emptyset_{sd}(i_{sd}) = f_1(i_{sd}) - i_{sd}^{ref} + k_1 e_{isd} \\ \emptyset_{sq}(i_{sd}) = f_2(i_{sq}) - i_{sq}^{ref} + k_2 e_{isq} \\ \emptyset_{rd}(i_{rd}) = f_3(i_{rd}) - i_{rd}^{ref} + k_3 e_{ird} \\ \emptyset_{rq}(i_{rq}) = f_4(i_{rq}) - i_{rq}^{ref} + k_4 e_{irq} \\ \emptyset_{\omega}(\omega) = f_5(\omega) - \dot{\omega}^{ref} + k_5 e_{\omega} \end{cases} \quad \dots \quad (37)$$

The super twisting algorithm defines the machine control voltages.

$$\begin{cases} v_{1sd} = -k_{10}\sqrt{|s_{isd}|}sign(s_{isd}) - k_{11}\int sign(s_{isd})dt \\ v_{1sq} = -k_{12}\sqrt{|s_{isq}|}sign(s_{isq}) - k_{13}\int sign(s_{isq})dt \\ v_{1rd} = -k_{14}\sqrt{|s_{ird}|}sign(s_{ird}) - k_{15}\int sign(s_{ird})dt \\ v_{1rq} = -k_{16}\sqrt{|s_{irq}|}sign(s_{irq}) - k_{17}\int sign(s_{irq})dt \\ C_{em} = -k_{18}\sqrt{|s_{\omega}|}sign(s_5) - k_{19}\int sign(s_{\omega})dt \end{cases} \quad \dots (38)$$

$$\begin{cases} \dot{s}_{isd} = \emptyset_{sd}(i_{sd}) - k_{10}\sqrt{|s_{isd}|}sign(s_{isd}) - k_{11}\int sign(s_{isd})dt \\ \dot{s}_{isq} = \emptyset_{sq}(i_{sq}) - k_{12}\sqrt{|s_{isq}|}sign(s_{isq}) - k_{13}\int sign(s_{isq})dt \\ \dot{s}_{ird} = \emptyset_{rd}(i_{rd}) - k_{14}\sqrt{|s_{ird}|}sign(s_{ird}) - k_{15}\int sign(s_{ird})dt \\ \dot{s}_{irq} = \emptyset_{rq}(i_{rq}) - k_{16}\sqrt{|s_{irq}|}sign(s_{irq}) - k_{17}\int sign(s_{irq})dt \\ \dot{s}_{\omega} = \emptyset_{\omega}(\omega) - k_{18}\frac{1}{J}\sqrt{|s_{\omega}|}sign(s_{\omega}) - k_{19}\frac{1}{J}\int sign(s_{\omega})dt \end{cases} \quad \dots (39)$$

By making a change of variable, we have the following new equations.

$$\begin{cases} \dot{s}_{isd} = \emptyset_{sd}(i_{sd}) - k_{10}\sqrt{|s_{isd}|}sign(s_{isd}) - s_{isd2} \\ \dot{s}_{isq} = \emptyset_{sq}(i_{sq}) - k_{12}\sqrt{|s_{isq}|}sign(s_{isq}) - s_{isq2} \\ \dot{s}_{ird} = \emptyset_{rd}(i_{rd}) - k_{14}\sqrt{|s_{ird}|}sign(s_{ird}) - s_{ird2} \\ \dot{s}_{irq} = \emptyset_{rq}(i_{rq}) - k_{16}\sqrt{|s_{irq}|}sign(s_{irq}) - s_{irq2} \\ \dot{s}_{\omega} = \emptyset_{\omega}(\omega) - k_{18}\frac{1}{J}\sqrt{|s_{\omega}|}sign(s_{\omega}) - s_{\omega 2} \end{cases} \quad \dots (40)$$

$$\begin{cases} \dot{s}_{isd2} = k_{11}sign(s_{isd}) \\ \dot{s}_{isq2} = k_{13}sign(s_{isq}) \\ \dot{s}_{ird2} = k_{15}sign(s_{ird}) \\ \dot{s}_{irq2} = k_{17}sign(s_{irq}) \\ \dot{s}_{\omega 2} = k_{19}\frac{1}{J}sign(s_{\omega}) \end{cases} \quad \dots (41)$$

We define the following vector:

$$\delta_i = \left[\sqrt{|s_i|}sign(s_i) \quad s_i\right]^T \quad \dots (42)$$

With $i = [i_{sd} \quad i_{sq} \quad i_{rd} \quad i_{rq} \quad \omega]^T$
The derivative of δ_i is given by

$$\dot{\delta}_i = |s_i|^{\frac{1}{2}}\left[\frac{-k_i}{2}\sqrt{|s_i|}sign(s_i) + \frac{1}{2}s_i + \emptyset_i(i) \quad -s_{i2}\sqrt{|s_i|}sign(s_i)\right]^T \quad \dots (43)$$

The equation can be rewritten in this way.

$$\dot{\delta}_i = |s_i|^{\frac{1}{2}}(A_i\delta_i + \rho_i) \quad \dots (44)$$

With $A_i = \begin{bmatrix} -\frac{k_{i1}}{2} & \frac{1}{2} \\ -k_{i2} & 0 \end{bmatrix}$, $\rho_i = \begin{bmatrix} \frac{1}{2}\emptyset_i(i) \\ 0 \end{bmatrix}$

Consider the following external perturbation bound. $|\rho_i| = \varepsilon\sqrt{|s_i|}$ with $\varepsilon > 0$, a positive constant.
Let the Lyapunov function be defined by

$$V(\delta_i) = \delta_i{}^T P_i \delta_i \quad \dots (45)$$

With $P_i = \frac{1}{2}\begin{bmatrix} 4k_{i2} + k_{i1} & -k_{i1} \\ -ki1 & 2 \end{bmatrix}$

The derivative of the Lyapunov function is given by

$$\dot{V}_i(\delta_i) = \sqrt{|s_i|}\delta_i{}^T(A_i^T P_i + P_i A_i)\delta_i + 2\sqrt{|s_i|}\delta_i{}^T P_i \rho_i \quad \dots (46)$$

The derivative of the Lyapunov function can be written in the following form.

$$\dot{V}_i(\delta_i) = \sqrt{|s_i|}\delta_i{}^T H_i \delta_i \quad \dots (47)$$

With

$H_i = \frac{k_{i1}}{2}\begin{bmatrix} k_{i2}^2 + 2k_{i2} - \delta_i\left(k_{i1} + 4\frac{k_{i2}}{k_{i1}}\right) & -k_{i1} \\ -(k_{i1} - \delta_i) & 1 \end{bmatrix}$ The matrix H_i is positive if the coefficients k_{i1} and k_{i2} meet the following conditions:

$$k_{i1} > 2\delta_i \quad \dots (48)$$

$$k_{i2} > \frac{1}{2}\frac{k_{i1}^2(\delta_i - k_{i1})}{k_{i1} - 2\delta_i} \quad \dots (49)$$

The coefficients of the controllers are chosen to account for these conditions, ensuring the system's stability. However, the performance of the controllers strongly depends on the values of the coefficients, which is why the PSO algorithm calculates the optimum coefficients.

D. PSO Method

The inductance's dependence on the magnetising current prevents a direct calculation of the controller gain. We employ the PSO method because it enables us to find the system's ideal coefficients within a narrow time window. The PSO algorithm will be used to determine the corresponding coefficients for the five controllers required by the proposed system. The formulas used to determine each object's position and speed are as follows:

$$V_{i+1} = \varepsilon_1 V_i + \varepsilon_2(x_{ip} - x_i) + \varepsilon_p(x_g - x_i) \quad \dots (50)$$

$$x_{i+1} = x_i + V_{i+1} \quad \dots (51)$$

Where the constants are the best position of an i^{th} particle from the first iteration and the global position of the swarm, respectively, the flowchart of this algorithm is given in Figure. 2.

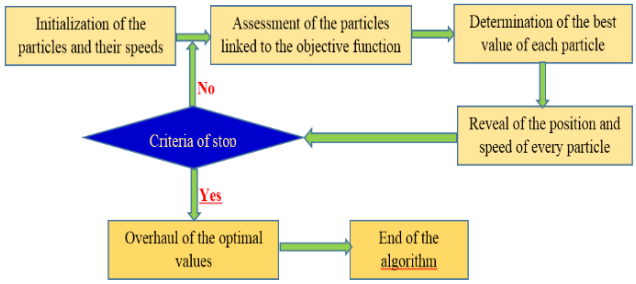

[Fig.2: Flowchart of the PSO Algorithm]

Published By:
Blue Eyes Intelligence Engineering
and Sciences Publication (BEIESP)

E. Synthesis of Observer

In this section, we will synthesise an interconnected Luenberger observer that can reconstruct rotational speed from measured currents and voltages of the rotor and the stator of a saturated DFIM.

Equation (13) for the machine can be expressed as follows.

$$\begin{cases} \frac{di_{sd}}{dt} = -a_1 i_{sd} + (a\omega_r + \omega_s) i_{sq} + a_3 i_{rd} + a_5 \omega_r i_{rq} + b_1 v_{sd} - b_3 v_{rd} \\ \frac{di_{sq}}{dt} = (a\omega_r + \omega_s) i_{sd} - a_1 i_{sq} - a_5 \omega_r i_{rd} + a_3 i_{rq} + b_1 v_{sq} - b_3 v_{rq} \\ \frac{di_{rd}}{dt} = a_4 i_{sd} - a_6 \omega_r i_{sq} - a_2 i_{rd} + \left(\omega_s - \frac{\omega_r}{\sigma}\right) i_{rq} - b_3 v_{sd} + b_2 v_{rd} \\ \frac{di_{rq}}{dt} = -a_6 \omega_r i_{sd} + a_4 i_{sq} - \left(\omega_s - \frac{\omega_r}{\sigma}\right) i_{rd} - a_2 i_{rq} - b_3 v_{sq} + b_2 v_{rq} \\ \frac{d\omega}{dt} = m_1 (i_{sq} i_{rd} - i_{sd} i_{rq}) - m_2 \omega \end{cases} \quad \dots (52)$$

With $a = \frac{1-\sigma}{\sigma}$, $a_1 = \frac{R_s}{\sigma l_s}$, $a_2 = \frac{R_r}{\sigma l_r}$, $a_3 = \frac{R_r M_{sr}}{\sigma l_s l_r}$, $a_4 = \frac{R_s M_{sr}}{\sigma l_s l_r}$, $a_5 = \frac{M_{sr}}{\sigma l_s}$, $a_6 = \frac{M_{sr}}{\sigma l_r}$, $b_1 = \frac{1}{\sigma l_s}$, $b_2 = \frac{1}{\sigma l_r}$, $b_3 = \frac{M_{sr}}{\sigma l_s l_r}$, $\sigma = \frac{1-M_{sr}^2}{l_s l_r}$

This model is broken down into two subsystems, the first of which is as follows:

$$\begin{cases} \dot{X}_1 = A_1(X_2) X_1 + g_1(u, y, X_1, X_2) \\ y_1 = C_1 X_1 \end{cases} \quad \dots (53)$$

With

$X_1 = [i_{sd}, \omega]^T$

$$A_1(X_1) = \begin{bmatrix} -a_1 & 0 \\ -m_1 i_{rq} & -m_2 \end{bmatrix},$$

$$g_1(u, y, X_1, X_2) = \begin{bmatrix} (a\omega_r + \omega_s) i_{sq} + a_3 i_{rd} + a_5 \omega_r i_{rq} + b_1 v_{sd} - b_3 v_{rd} \\ m_1 (i_{sq} i_{rd}) \end{bmatrix},$$

$C_1 = [0 \quad 1]$

The following equation gives the second subsystem:

$$\begin{cases} \dot{X}_2 = A_2(X_1) X_2 + g_2(u, y, X_1, X_2) \\ y_2 = C_2 X_2 \end{cases} \quad \dots (54)$$

With

$, X_2 = [i_{sq}, i_{rd}, i_{rq}]^T$

$$A_2(X_1) = \begin{bmatrix} -a_1 & -a_5 \omega_r & a_3 \\ -a_6 \omega_r & -a_2 & \left(\omega_s - \frac{\omega_r}{\sigma}\right) \\ a_4 & -\left(\omega_s - \frac{\omega_r}{\sigma}\right) & -a_2 \end{bmatrix}$$

$$C_2 = [1 \quad 0 \quad 0]$$

$$g_2(u, y, X_1, X_2) = \begin{bmatrix} (a\omega_r + \omega_s) i_{sd} + b_1 v_{sq} - b_3 v_{rq} \\ a_4 i_{sd} - b_3 v_{sd} + b_2 v_{rd} \\ -a_6 \omega_r i_{sd} - b_3 v_{sq} + b_2 v_{rq} \end{bmatrix},$$

The observer copies the dynamics of the system while correcting the observation errors, which gives us the following form:

$$\begin{cases} \dot{H}_1 = B_1(H_2) H_1 + f_1(u, y, H_1, H_2) + G(y_1 - \hat{y}_1) \\ \hat{y}_1 = C_1 H_1 \end{cases} \quad \dots (55)$$

$$\begin{cases} \dot{H}_2 = B_2(H_1) H_2 + f_2(u, y, H_1, H_2) + K(y_2 - \hat{y}_2) \\ \hat{y}_2 = C_2 H_2 \end{cases} \quad \dots (56)$$

with $\dot{H}_1 = [\hat{\imath}_{sd}, \hat{\omega}]^T$, $B_1(H_2) = \begin{bmatrix} -a_1 & 0 \\ -m_1 \hat{\imath}_{rq} & -m_2 \end{bmatrix}$,

$$f_1(u, \hat{y}, H_1, H_2) = \begin{bmatrix} (a\omega_r + \omega_s) \hat{\imath}_{sq} + a_3 \hat{\imath}_{rd} + a_5 \omega_r \hat{\imath}_{rq} + b_1 v_{sd} - b_3 v_{rd} \\ m_1 (\hat{\imath}_{sq} \hat{\imath}_{rd}) \end{bmatrix},$$

$H_2 = [\hat{\imath}_{sq}, \hat{\imath}_{rd}, \hat{\imath}_{rq}]^T$,

$$B_2(H_1) = \begin{bmatrix} -a_1 & -a_5 \omega_r & a_3 \\ -a_6 \omega_r & -a_2 & \left(\omega_s - \frac{\omega_r}{\sigma}\right) \\ a_4 & -\left(\omega_s - \frac{\omega_r}{\sigma}\right) & -a_2 \end{bmatrix},$$

$$f_2(u, \hat{y}, H_1, H_2) = \begin{bmatrix} (a\omega_r + \omega_s) \hat{\imath}_{sd} + b_1 v_{sq} - b_3 v_{rq} \\ a_4 \hat{\imath}_{sd} - b_3 v_{sd} + b_2 v_{rd} \\ -a_6 \omega_r \hat{\imath}_{sd} - b_3 v_{sq} + b_2 v_{rq} \end{bmatrix},$$

$$G = \begin{bmatrix} G_1 \\ G_2 \end{bmatrix}, K = \begin{bmatrix} K_1 \\ K_2 \\ K_3 \end{bmatrix}$$

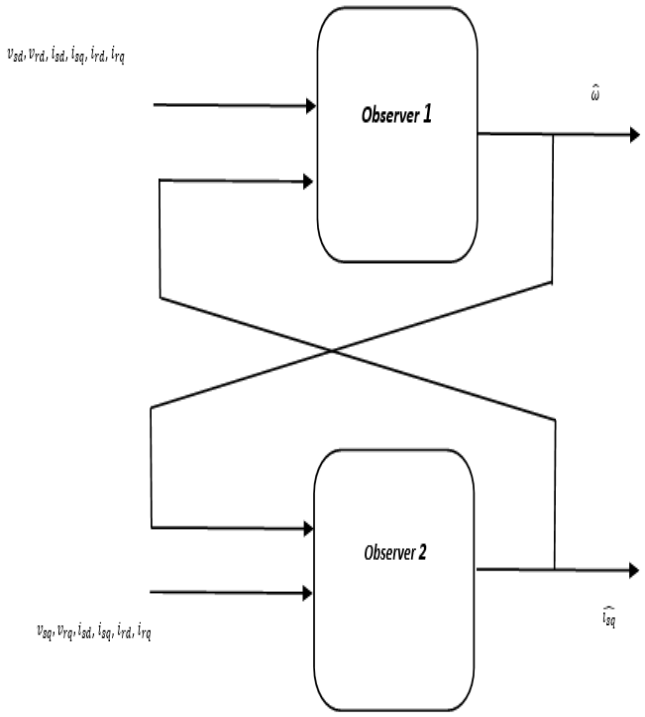

[Fig.3: Internal Structure of the Observer]

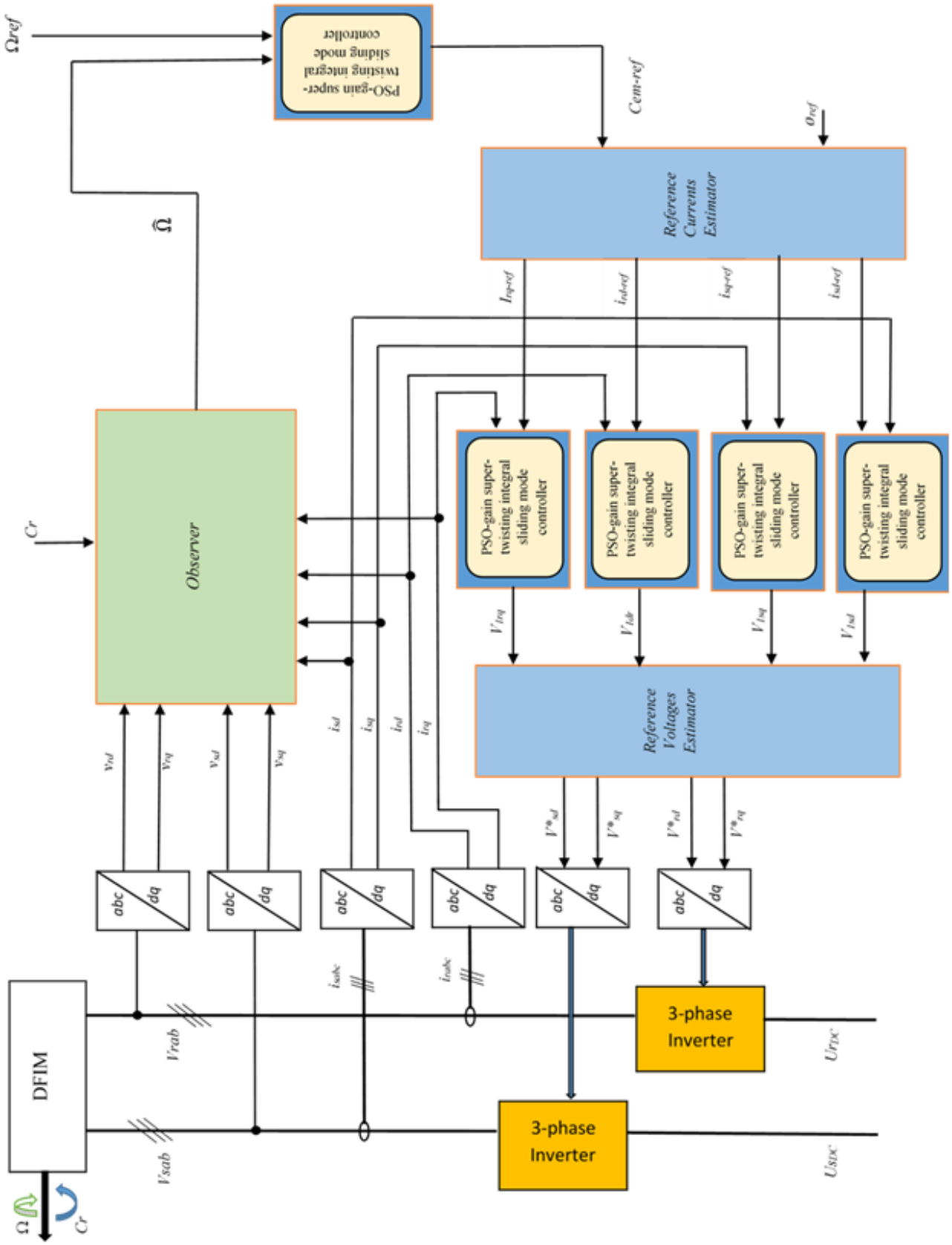

[Fig.4: Global Structure of PSO-Gain Integral Super-Twisting Control of DFIM]

III. RESULTS AND DISCUSSION

The coefficients were calculated with 150 iterations on 100 particles. For each iteration, the system's performance is evaluated, and the objective function is shown in Figure 5. With the objective function being satisfactory and the curve tending towards zero, a verification of the flux orientation was then carried out, as shown in Figure 6 below, which indicates that the quadrature flux is close to zero.

Retrieval Number: 100.1/ijitee.F109514060525
DOI: 10.35940/ijitee.F1095.14070625
Journal Website: www.ijitee.org

Published By:
Blue Eyes Intelligence Engineering
and Sciences Publication (BEIESP)

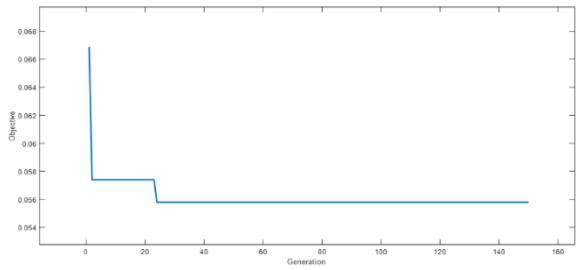

[Fig.5: Curve Illustrating Goal Attainment as a Function of Iterations]

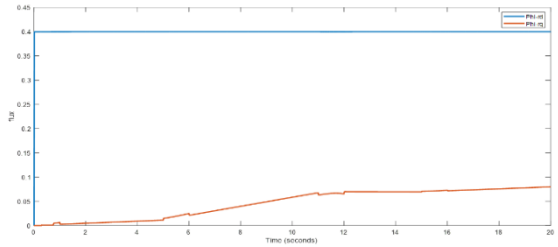

[Fig.6: Curve Illustrating Flow Orientation Along the Direct Axis]

A. PSO-gain Super-Twisting Integral Sliding Mode Controller for Sensor-Less Speed Control of Saturated DFIM

To demonstrate the robustness of the control system, a reference speed profile is applied to the machine at no load and compared with the speed observed on the machine shaft. The speed and load torque references consider all trajectories required to analyse the dynamic performance of the entire control law. The initial values of mechanical speed and load torque are held at 0 to allow flow to establish itself in the machine. At t=0.75s, the machine speed is increased to 20 rad/s and remains constant until 5s. This initial phase is used to test and evaluate the dynamic performance of the control law at low speeds. The machine is then accelerated to a high speed (100 rad/s). This second phase aims to test the performance of the control law during a large speed transient and at high speed. The machine is then rapidly decelerated to reach a low negative speed (-1 rad/s) at t=12s, which remains constant until t=15s with load torque as displayed in Figure 7. This phase highlights the performance of the control law in the critical "very low frequency" zone. Finally, the trajectories bring the machine into the low-speed zone.

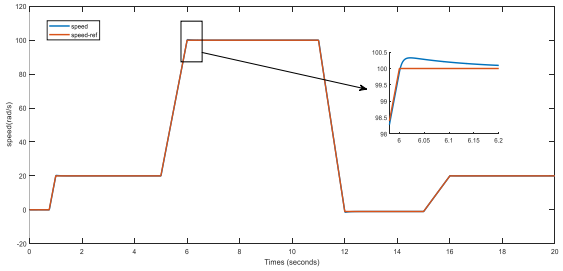

[Fig.7: Speed and Reference Speed Curves with PSO-Gain Integral Super-Twisting]

The super-twisting integral is also compared to the classic super-twisting applied to the previous machine, which has the same set-point speed profile. We can see from Figure 8 that the super-twisting integral converges more, and the deviations from the set point curve are minimal. At low speeds, i.e. from 0 to 20rad/s, the super-twisting succeeds in the control, and overshoots are almost non-existent. From 20 to 100rad/s, the super-twisting controller does not succeed like the super-twisting integral controller in making the system converge perfectly. The difference in performance is also evident in the curves of the set-point tracking errors in Figures 9 and 10. In Figure 9, the set point tracking error in super-twisting speed takes on enormous proportions of up to 12.5rad/s, unlike in Figure 10, where the error rises to 1.2rad/s.

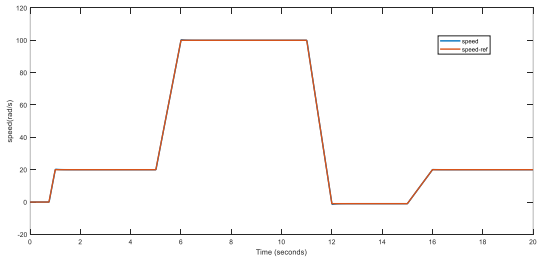

[Fig.8: Speed and Reference Speed Curves with PSO-Gain Super-Twisting]

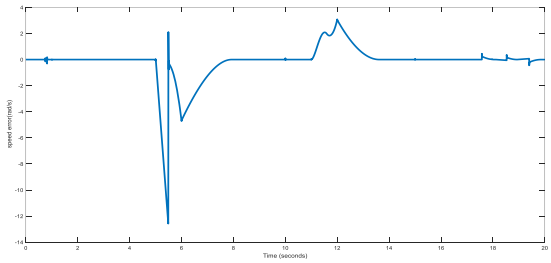

[Fig.9: Error Speed with PSO-Gain Super Twisting]

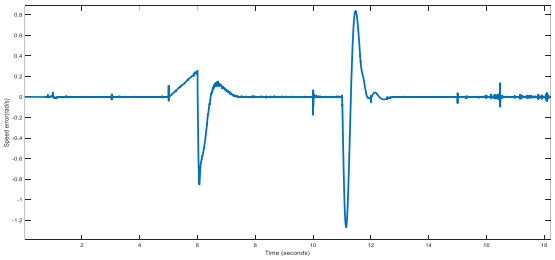

[Fig.10: Error Speed with PSO-Gain Integral Super Twisting]

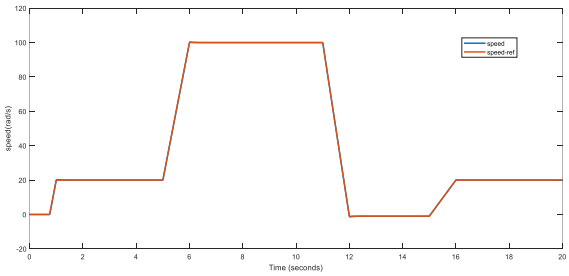

[Fig.11: Speed and Reference Speed Curves After Modification of Rotor Winding Resistances at +50% with PSO-Gain Super twisting]

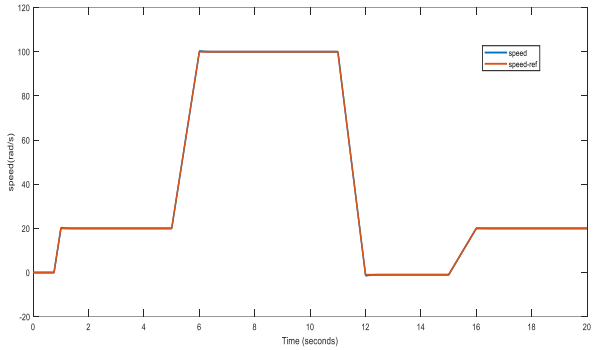

[Fig 12: Speed and Reference Speed Curves After Modification of Stator Winding Resistances at +50%]

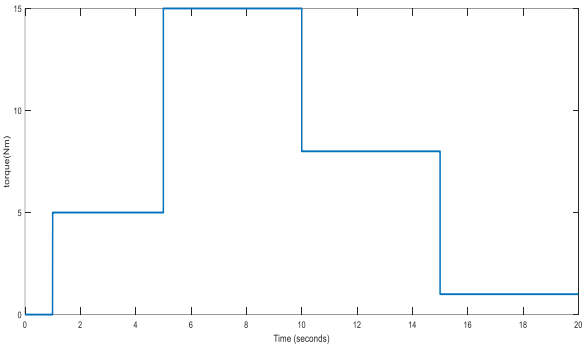

[Fig.13: Load Torque Profile for The Machine]

The internal resistance of the windings is a function of temperature and can also influence the controller (the controller coefficients are a function of these quantities). A robustness test to variations in resistive parameters is performed. The stator resistance varies by +50%, followed by the rotor resistance. Consider these variations. At the speed level, we observe insensitivity on vector control as presented in Figures 11 and 12.

Modifying the load torque also verifies the control's robustness. As a result, the machine is subjected to a time-varying torque profile, as shown in Figure 13. The control system remains systematically robust to load variations, as shown in Figure 14.

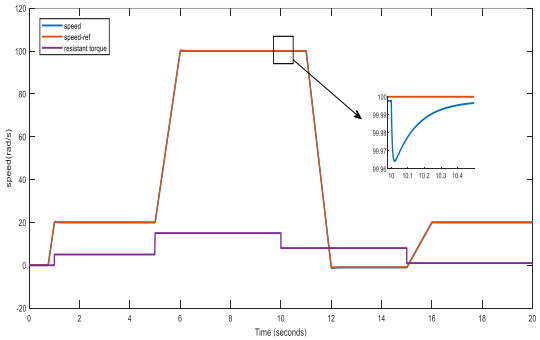

[Fig.14: Curve Illustrating Rotation Speed in the Presence of Variable Resistive Torque]

B. Synthesis of Observer

After synthesising the observer model, the PSO method determined the coefficients. The search for the optimal coefficients led us to the following objective function, as shown in Figure 15.

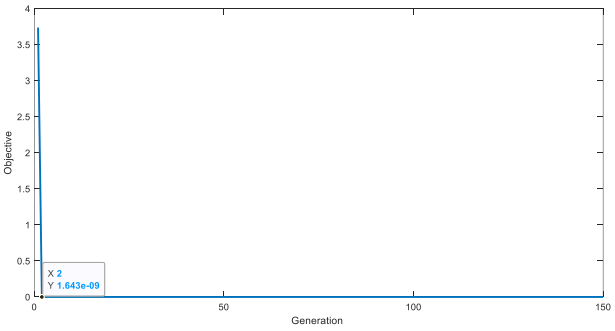

[Fig.15: Curve Illustrating Goal Attainment as a Function of Iterations]

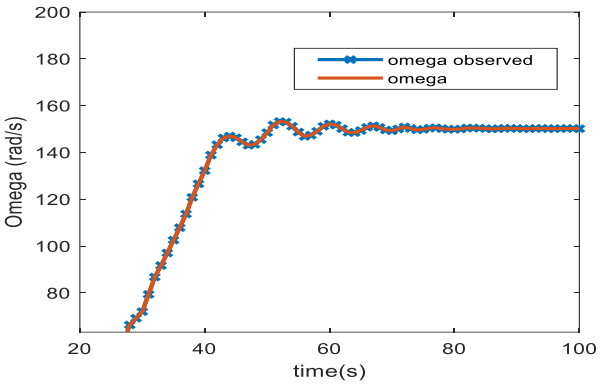

[Fig.16: Curves of the Speed and Engine and That Observed]

Figure 16 shows the velocity profile plotted jointly with that reconstructed by the observer. We can see the perfect convergence between the two curves, which is also demonstrated by Figure 17. The observation error, which is the difference between the two curves, is tiny. Thus, the observer, which is therefore designed, perfectly replaces the mechanical sensor in our system.

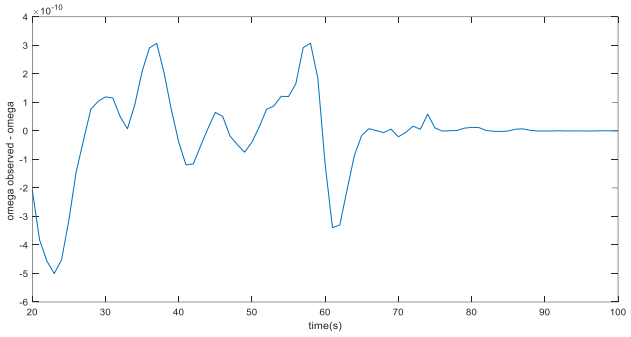

[Fig.17: Speed Observation Error Over Time]

IV. CONCLUSION

In this paper, we propose a sensorless speed control strategy for a saturated doubly-fed Induction machine (DFIM) using a PSO-gain super-twisting integral sliding mode controller for Sensorless speed control of saturated DFIMs. This approach addressed the challenges of speed control in a context of nonlinear dynamics, magnetic saturation, and the absence of mechanical sensors, while ensuring robustness and accuracy. the results obtained demonstrated the effectiveness of the proposed method. A comparison

Published By:
Blue Eyes Intelligence Engineering
and Sciences Publication (BEIESP)

between classic super twisting and integral super twisting was also carried out by applying both controls to the same machine following the same set point speed profile. We therefore highlighted that the results were better with the PSO-gain super twisting controllers. The PSO-gain Super-Twisting technique significantly reduced the chattering phenomenon while maintaining robustness against disturbances and parametric variations. The addition of the integral action improved the regulation accuracy by eliminating static errors and ensuring accurate tracking of the speed set point. Furthermore, the optimisation of the controller parameters by the particle swarm method achieved optimal performances, adapted to the specificities of the saturated DFIM. The simulations validated the proposed control's ability to operate under various conditions, including the presence of magnetic saturation and external disturbances.

This study opens promising perspectives for the application of robust and optimised control techniques in industrial systems using doubly fed induction machines. Future work could explore the practical implementation of this method on experimental platforms, as well as its extension to other types of machines or to multi-objective applications. This approach represents a significant step toward more efficient, robust, and cost-effective control systems for modern industrial applications.

DECLARATION STATEMENT

After aggregating input from all authors, I must verify the accuracy of the following information as the article's author.

- **Conflicts of Interest/ Competing Interests:** Based on my understanding, this article has no conflicts of interest.
- **Funding Support:** This article has not been funded by any organisations or agencies. This independence ensures that the research is conducted objectively and without external influence.
- **Ethical Approval and Consent to Participate:** The content of this article does not necessitate ethical approval or consent to participate with supporting documentation.
- **Data Access Statement and Material Availability:** The adequate resources of this article are publicly accessible.
- **Author's Contributions:** The authorship of this article is contributed equally to all participating individuals.

REFERENCES

1. L. Makhlouf and S. Lassaad. (2017). Steady state analysis of a doubly-fed induction generator. In the IEEE International Conference on Green Energy Conversion Systems. DOI: http://doi.org/10.4236/epe.2011.34050
2. P. K. Chaurasiya, V. Warudkar, and S. Ahmed. (2019) Wind energy development and policy in India: A review. In Energy Strategy Reviews. (Vol. 24, pp. 342– 357). DOI: https://doi.org/10.1016/j.esr.2019.04.010
3. Hiswe, E. Kenmoe. (2019). Optimisation of sensorless field-oriented control of an induction motor taking into account magnetic saturation. In Springer International Journal of Dynamics and Control. https://doi.org/10.1007/s40435-018-00503-8
4. Yuri Shtessel, Mohammed Taleb et Franck Plestan. (2012). A novel adaptive-gain supertwisting sliding mode controller: Methodology and application. In Elsevier Automatica (vol: 48, pp: 759–769). https://doi.org/10.1016/j.automatica.2012.02.024
5. Daniel Borice T., Clotaire T., Godpromesse K. (2025). Performance enhancement for a stand-alone wind energy conversion system using a super-twisting algorithm. In ELSEVIER Energy Reports (Vol: 13 pp: 1910–1926). DOI: https://doi.org/10.1016/j.egyr.2025.01.048
6. UTKIN, V. J. SHI. (1996). Integral sliding mode in systems operating under uncertain conditions. In Decision and Control, Proceedings of the 35th IEEE Conference (vol. 4, p.4591–4596, 27, 87). DOI: https://doi.org/10.1109/CDC.1996.577594
7. Federico Marini, Beata Walczac. (2015). Particle swarm optimisation (PSO): A tutorial. In ELSEVIER Chemometrics and Intelligent Laboratory Systems. (Vol 149, Pages 153-165). DOI: https://doi.org/10.1016/j.chemolab.2015.08.020
8. Wen, B., Burgos, R., Boroyevich, D., Mattavelli, P., & Shen, Z. (2017). AC stability analysis and dq frame impedance specifications in power-electronics-based distributed power systems. In IEEE Journal of Emerging and Selected Topics in Power Electronics. (vol: 5, Issue 4, pp: 1455-1465). DOI: https://doi.org/10.1109/JESTPE.2017.2728640
9. P.J. Tavner. (2004). Cross-magnetisation effects in electrical machines. In IEE Proceedings - Electric Power Applications (Vol 151, Issue 3). https://doi.org/10.1049/ip-epa:20040345
10. Hany M. Jabr, Narayan C. Kar. (2007). Effects of central and leakage flux saturation on the transient performances of a doubly-fed wind-driven induction generator. In ELSEVIER Journal of Electronic Power Systems Research. (No. 77, pp. 1019–1027). DOI: https://doi.org/10.1016/j.epsr.2006.08.034
11. Xinghuo Yu; Yong Feng; Zhihong Man. (2020). Terminal Sliding Mode Control – An Overview. In the IEEE Open Journal of Industrial Electronics. Society. (Vol 2, pp 36-52, ISSN 2644-1284). DOI: https://doi.org/10.1109/OJIES.2020.3040412
12. A.J. Koshkouei, K.J. Burnham, and A.S.I. Zinober (2005). Dynamic sliding mode control design. In IEE Proceedings- Control Theory and Applications. (Vol 152, Issue 4 ISSN:1359-7035). DOI: https://doi.org/10.1049/ip-cta:20055133
13. Burton, J. A., & Zinober, A. S. I. (1986). Continuous approximation of VSC. In International Journal of Systems Sciences, (vol: 17, pp: 875–885). DOI: https://doi.org/10.1080/00207728608926853
14. Levant, A. (1993). Sliding order and sliding accuracy in sliding mode control. In the *International Journal of Control*. (Vol: 58, pp: 1247–1263). DOI: https://doi.org/10.1080/00207179308923053

AUTHOR'S PROFILE

PABAME Frédéric, University of Dschang, Faculty of Sciences, Department of Physics, P.O. Box 96, Cameroon. Master of Science in Electronics in 2018. His research areas include the application of automation to diagnostics and sensorless control of electrical machines.

MFAH MBAKA Eustace, University of Dschang, IUT Fotso Victor, P.O. Box 134, Bandjoun, Cameroon. He is an Associate Professor of Electrical Engineering at the University of Dschang, Cameroon. He is currently the Deputy Director of the National Higher Polytechnic Institute of the University of Bamenda, Cameroon. He has over 26 years of experience in teaching and research at two State Universities and has published more than 20 articles. He is a researcher with a focus on standalone or hybrid power systems using renewable energy and conventional resources.